Eight-Channel Silicon-Photonic Wavelength Division Multiplexer With 17 GHz Spacing

Dvir Munk, Moshe Katzman, Yuri Kaganovskii, Naor Inbar, Arijit Misra ⓘ, Mirit Hen, Maayan Priel,
Moshe Feldberg, Maria Tkachev, Arik Bergman ⓘ, Menachem Vofsi, Michael Rosenbluh ⓘ,
Thomas Schneider, and Avi Zadok ⓘ

Abstract—**Dense wavelength division multiplexers are key components of data communication networks. This paper presents a silicon-photonic eight-channel multiplexer device with a channel spacing of only 0.133 nm (17 GHz). Devices were fabricated in a commercial silicon foundry, in 8" silicon-on-insulator wafers. The device layout consists of seven unbalanced Mach–Zehnder interferometers in a cascaded tree topology, and each interferometer unit also includes a nested ring resonator element. The transfer function of each unit is that of a maximally flat, autoregressive, moving-average filter. The devices are characterized by uniform passbands, sharp spectral transitions between pass and stop bands, and strong out-of-band rejection. The worst-case optical power crosstalk is −22 dB. The proper function of the device requires careful control of optical phase delays over 14 distinct optical paths. Post-fabrication trimming of phase delays was performed through local illumination of a photo-sensitive upper cladding layer of chalcogenide glass. The de-multiplexing of three adjacent QAM-16, 40 Gbit/s wavelength-division channels was successfully demonstrated. The devices are applicable in data communication and in integrated-photonic processing of radio-over-fiber waveforms.**

Index Terms—**Silicon photonics, optical communication, wavelength division multiplexing, photonic integrated circuits, data communication, chalcogenide glasses, optical filters.**

D. Munk, M. Katzman, M. Hen, M. Priel, A. Bergman, and A. Zadok are with the Faculty of Engineering and Institute for Nano-Technology and Advanced Materials, Bar-Ilan University, Ramat Gan 5290002, Israel (e-mail: dvirmu@gmail.com; moshekatzman111@gmail.com; mirithen071110@gmail.com; lmaayanl@gmail.com; bergman.arik@gmail.com; avinoam.zadok@biu.ac.il).

Y. Kaganovskii and M. Rosenbluh are with the Department of Physics and Institute for Nano-Technology and Advanced Materials, Bar-Ilan University, Ramat Gan 5290002, Israel (e-mail: yuri.kaganovsky@biu.ac.il; rosenbluh@biu.ac.il).

N. Inbar and M. Vofsi are with the Tower-Jazz Semiconductors, Migdal Ha'Emek 2310502, Israel (e-mail: naorin@towersemi.com; nachi@towersemi.com).

A. Misra and T. Schneider are with the Institute for High-Frequency Technology, Technical University of Braunschweig, 38016 Braunschweig, Germany (e-mail: arijit.misra@ihf.tu-bs.de; thomas.schneider@ihf.tu-bs.de).

M. Feldberg and M. Tkachev are with the Institute for Nano-Technology and Advanced Materials, Bar-Ilan University, Ramat Gan 5290002, Israel (e-mail: moshe.feldberg@biu.ac.il; maria.tkachev@biu.ac.il).

Color versions of one or more of the figures in this paper are available online at http://ieeexplore.ieee.org.

Digital Object Identifier 10.1109/JSTQE.2019.2904437

I. INTRODUCTION

PHOTONIC integrated circuits are widely regarded as key enabling technology for sustaining the growth of data communication. Silicon-on-insulator (SOI) is a favorable material platform for the realization of passive photonic devices, due to a broad transparency window, mature fabrication technology, comparatively tight confinement of light in high-contrast waveguides, and compatibility with electronic integrated circuits [1], [2]. A common and significant task of silicon-photonic devices is wavelength-division multiplexing, de-multiplexing and filtering of communication channels [3]–[6]. Silicon wavelength-division multiplexers are realized based on Mach-Zehnder interferometers (MZIs) [7], coupled ring resonators [8], arrayed waveguide gratings (AWGs) [9]–[13] and echelle gratings [13]–[16]. Device performance metrics include large port count, narrow transmission bandwidth, uniform in-band transmission, strong out-of-band rejection, and sharp spectral transitions between pass and stop bands.

Most dense wavelength division multiplexing (DWDM) SOI devices rely on interference among multiple optical paths. Their proper function mandates the precise definition of the optical phase delay along each path. Unfortunately, nanometer-scale tolerances in the widths and heights of silicon waveguides often induce excessive uncertainty in optical phases. Phase variations scale with waveguides lengths. Hence, DWDM devices with a narrow free spectral range (FSR) are more susceptible to phase delay errors. In most cases, the correct transfer function cannot be obtained with open-loop fabrication, and some form of post-fabrication tuning is necessary.

Optical phase delays may be adjusted using continuous active methods, such as the injection of current to p-n junctions across waveguides [17], [18], or local heating through metallic or implanted silicon resistors [19], [20]. Active tuning provides maximum flexibility, but requires continuous feedback and increases the complexity of device fabrication and operation. In addition, continuous heating increases power consumption. In many cases, the device is designed to carry out a single function with no reconfiguration, and the operation temperature may be fixed. Under such conditions, one-time, permanent trimming of the device response is preferable [21]–[24]. The complexity of all tuning protocols, one-time or continuous, scales with the number of wavelength channels. Due to difficulties associated with phase control, many silicon-photonic DWDM devices

are restricted to only four channels, and/or comparatively wide channel spacing of 100 GHz or more, and/or compromised response metrics.

In this work, we report a silicon-photonic eight-channel DWDM device with a narrow spacing of only 0.133 nm (17 GHz) between adjacent spectral channels. The device consists of seven filter stages in a cascaded tree topology. Each stage includes a MZI unit with an unbalanced differential group delay, and a ring resonator nested in its shorter arm. The frequency response of each stage is that of a maximally-flat, auto-regressive, moving-average (ARMA) filter [25]. Compared with finite impulse response elements, such as MZIs-only layouts or AWGs, the ARMA filters provide more uniform passbands, stronger out-of-band rejection and sharper spectral transitions with fewer waveguide paths [25]. Multi-stage ARMA DWDM devices in silicon were successfully demonstrated in several previous works [26], [27]. However, the relative complexity of the layout restricted these devices to four-port operation, wide channel spacing and elevated crosstalk levels. MZIs with nested ring resonators were also used in linearized silicon-photonic electro-optic modulators [28].

The large number of output ports and the narrow FSR raise a formidable challenge in phase delay trimming. To that end, patches of a thin upper cladding layer of As_2Se_3 chalcogenide glass were deposited on top of the silicon waveguides in select locations [29]–[31]. The illuminations of the upper cladding with a focused laser beam locally modifies its refractive index, and with higher exposure can even result in the removal of the cladding layer [32], [33]. Both mechanisms modify the local effective index of the guided optical mode, and adjust the overall phase delay in small controllable increments. Successive tuning steps were taken, subject to closed-loop monitoring of transfer functions, until the target response was reached.

All 14 phase delay degrees of freedom were corrected sequentially according to a tuning procedure. No cross-interference was observed in the adjustment of different paths. The full width at half maximum of the transfer function in each output port is 0.11 nm. Out-of-band crosstalk is particularly low: -28 dB on average, with a worst-case upper bound of -22 dB. Following the trimming procedure, the device response remained stable over months. Lastly, three adjacent wavelength-division channels, with 17 GHz spacing between their central frequencies, were successfully de-multiplexed at the device output. Each channel carried data in quadrature-amplitude modulation-16 (QAM-16) format and 10 Gbd/s rate (40 Gbit/s). The spectral efficiency of the transmitted data was 2.35 bit/s per Hz, in a single polarization.

The design of the DWDM device is presented in Section II. Device fabrication, tuning and testing are reported in Section III. A data transmission experiment is described in Section IV, and concluding remarks are given in Section V. Results were briefly presented at a recent conference [34].

II. DESIGN OF WAVELENGTH-DIVISION MULTIPLEXING DEVICE

The design of the DWDM device relies on the mathematical equivalence between the transfer functions of optical filter ele-
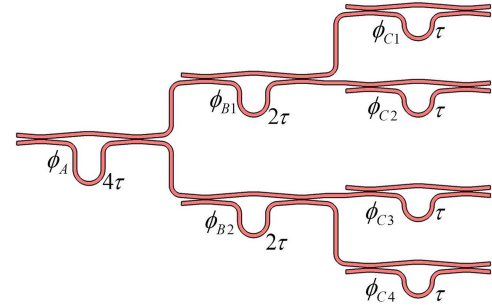

Fig. 1.   Schematic illustration of an eight-channel dense wavelength division multiplexer device, based on cascaded Mach-Zehnder interferometers. Differential phase and group delays are noted for each stage (see main text).

ments and those of digital filters [25]. The transfer function of an unbalanced MZI stage is analogous to that of a single-stage, finite-impulse-response (or moving-average) digital filter. As such, it is completely defined by the location of a single zero-transmission point, (or 'zero' for short), in the complex Z plane [25]. Similarly, the transfer function of a photonic-integrated ring resonator is equivalent to that of a first-order infinite-impulse-response digital filter. Such filters are also referred to as auto-regressive [25]. Their response is entirely determined by the location of a single pole in the complex Z plane [25], where the transfer function approaches infinity. The response of the most general digital filter may be expressed in terms of sets of zero and pole locations [25]. Designs that exhibit both zeros and poles are often referred to as ARMA filters [25].

A. Cascaded Mach-Zehnder Interferometers

The DWDM layout consists of seven filter stages, each based on an unbalanced MZI. Let us first examine the response of a filter comprised of MZIs only, with no resonators (Fig. 1). All MZI units are built with equal 50/50 directional couplers at both ends. Incident light is coupled to the upper input port of the first MZI (stage A). The differential group delay between the two arms of this MZI is the largest: it equals 4τ, where τ represents a fundamental group delay unit. We denote the differential phase delay between the two arms of the stage A MZI at a reference optical frequency ω_0 as ϕ_A.

The upper output port of MZI A is connected to the lower input port of a second MZI, denoted as B_1. The lower output port of MZI A is connected to the upper input port of MZI B_2 (see Fig. 1). MZI units B_k, $k = 1, 2$, constitute the second (B) filtering stage of the device. Both are characterized by differential group delays of 2τ. We denote their respective differential phase delays at ω_0 as ϕ_{Bk}. Lastly, the four output ports of the B-stage MZIs are connected to input ports of four final MZIs, which make up the final C-stage of the device (Fig. 1). We refer to the four MZIs as C_i, with $i = 1 \ldots 4$. The differential group delays in all four equals the basic unit τ, and their differential phase delays at ω_0 are denoted by ϕ_{Ci}.

The overall transfer functions from the common input port of the device to each of the eight output ports may be brought to
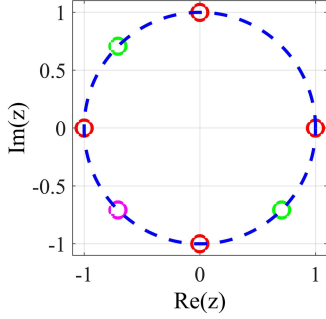
Fig. 2. Locations of zeros of the Z-domain transfer function of output port 1 of a cascaded Mach-Zehnder interferometer wavelength-division multiplexer device (circles). Four locations correspond to stage *A* (red), two to stage *B* (green), and one to stage *C* (magenta). Zeros are located at normalized frequencies that are integer multiples of $\pi/4$. The passband is centered at a normalized frequency of $\pi/4$, where no zero is placed.

TABLE I
CHOICE OF DIFFERENTIAL PHASE DELAYS WITHIN A CASCADED
MACH-ZEHNDER INTERFEROMETERIC WAVELENGTH
DIVISION MULTIPLEXER

Filter unit	Differential phase delay
A	$\phi_A = 0$
B_1	$\phi_{B1} = 3\pi/2$
B_2	$\phi_{B2} = 0$
C_1	$\phi_{C1} = 3\pi/4$
C_2	$\phi_{C2} = \pi/4$
C_3	$\phi_{C3} = \pi/2$
C_4	$\phi_{C4} = 0$

the following form [25]:

$$h_l(Z) = \prod_{m=1}^{7} \left(z_{l,m} - Z^{-1} \right). \qquad (1)$$

Here $h_l(Z)$ denotes the Z-domain transfer function from the input to output port $l = 1 \ldots 8$, and $z_{l,m}$ is the mth zero of $h_l(Z)$, $m = 1 \ldots 7$. The locations of its seven zeros completely define each of the eight transfer functions. The zeros, in turn, are determined by choices of the seven differential phases: ϕ_A, ϕ_{Bk} and ϕ_{Ci}. All zeros are located on the unit circle of the complex Z plane: $z_{l,m} = \exp(j\phi_{l,m})$.

The device design aims to locate all zeros at integer multiples of $\pi/4$ radians, $\phi_{l,m} = n\pi/4$, $n \in \{1 \ldots 8\}$, with the following distinction among output ports: For each output l, zeros are located at all $n \neq l$ positions, and no zero is placed at $n = l$ (see Fig. 2 for illustration). The passband of output port l is centered at normalized frequency $l\pi/4$. One possible choice of the seven differential phases is listed in Table I.

Figure 3 shows the calculated normalized-frequency power transfer functions $|h_l|^2$, obtained by substituting $Z = \exp(j\Omega)$. The input spectrum is divided into eight periodic bands, each routed to a different output port. The proper functioning of the device critically depends on accurate adjustments of the differential phase delays within all seven MZI units.
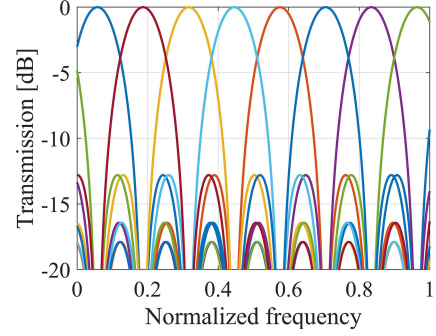

Fig. 3. Calculated normalized-frequency transfer functions of the eight output ports of a cascaded Mach-Zehnder interferometer, wavelength-division multiplexer device.
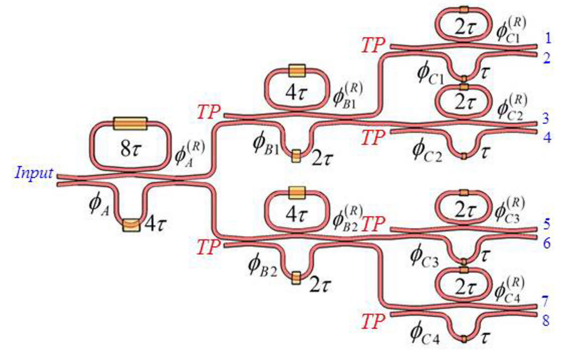

Fig. 4. Schematic illustration of an eight-channel dense wavelength-division multiplexer device, based on cascaded Mach-Zehnder interferometers with nested ring resonators. The transfer function of each of the seven filter stages is that of a maximally-flat auto-regressive, moving-average filter. Orange-colored patches denote the locations of photo-sensitive upper cladding of chalcogenide glass (see below). Differential group and phase delays are noted for each Mach-Zehnder stage. One-pass group and phase delays are noted for each resonator (see main text). TP: test port.

B. Auto-Regressive Moving-Average Filter Stages

Figure 4 shows a schematic illustration of a DWDM device, in which each of the seven constituent MZI units also includes a nested ring resonator in its shorter arm. The single-path group delay along each ring resonator is chosen as twice longer than the differential group delay between the host MZI arms [25]: 8τ, 4τ and 2τ for filter units in the *A*, *B* and *C* stages, respectively (see Fig. 4).

Consider for example filter unit C_4. Let us denote the single-path phase delay along its ring resonator at ω_0 as $\phi_{C4}^{(R)}$. The Z-domain transfer function between the upper input port and the upper output port of the unit is given by [25]:

$$h_{C4}^{(1)}(Z) = \frac{1}{2} \exp\left(-j\phi_{C4}^{(R)}\right) \frac{\rho \exp\left(j\phi_{C4}^{(R)}\right) - Z^{-2}}{1 - \rho \exp\left(j\phi_{C4}^{(R)}\right) Z^{-2}} - \frac{1}{2} Z^{-1}$$

$$= \frac{1}{2} \frac{\rho - Z^{-1} - \exp\left(j\phi_{C4}^{(R)}\right) Z^{-2} + \rho \exp\left(j\phi_{C4}^{(R)}\right) Z^{-3}}{1 - \rho \exp\left(j\phi_{C4}^{(R)}\right) Z^{-2}}.$$
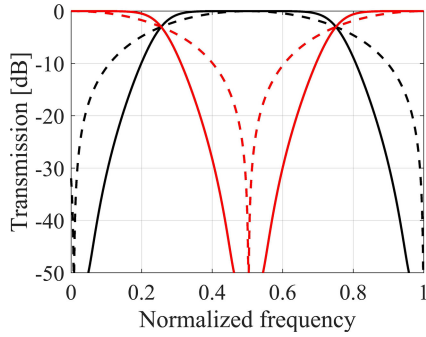
$$(2)$$

Fig. 5. Calculated normalized-frequency transfer functions of a single-stage auto-regressive, moving-average filter (solid lines), alongside those of a single-stage Mach-Zehnder interferometer filter (dashed line). Black (red) traces correspond to the upper (lower) output port of the filter stages.

Here ρ denotes the fraction of the optical field magnitude that is directed to the through port of the directional coupler that forms the ring resonator [25]. The complementary transfer function to the lower output port is given by [25]:

$$
h_{C4}^{(2)}(Z)
$$

$$
= \frac{j}{2} \frac{\rho + Z^{-1} - \exp\left(j\phi_{C4}^{(R)}\right) Z^{-2} - \rho \exp\left(j\phi_{C4}^{(R)}\right) Z^{-3}}{1 - \rho \exp\left(j\phi_{C4}^{(R)}\right) Z^{-2}}
$$

(3)

For $\rho = 1/3$ and $\phi_{C4}^{(R)} = \pi$, the Z-domain responses of Eq. (2) and Eq. (3) become those of maximally-flat, third-order Butterworth filters [25]. The passbands of the two filters are centered at normalized frequencies $\Omega/(2\pi)$ of 0.5 and 0, respectively [25]. Fig. 5 shows the calculated normalized-frequency power transfer functions of the two output ports, alongside those of a simple MZI. The incorporation of the ring resonator, and proper choices of coupling ratio and phase delay, provide more uniform pass-bands, stronger out-of-band rejection, and sharper spectral transitions.

The transfer functions of all seven ARMA units can be similarly calculated. A value of $\rho = 1/3$ is chosen for all. The phase delays at ω_0 vary among the seven resonators, in order to retain the different central transmission frequencies of all output ports. The phase delays in all MZIs and resonators are summarized in Table II. Fig. 6 shows the calculated normalized-frequency power transfer functions of all output ports of a cascaded ARMA filter DWDM device. The calculations also include the effect of propagation losses in our specific waveguides (see detailes in Section III). The corresponding transfer functions of a MZIs-only device (Fig. 3) are drawn again for comparison. The benefits of the ARMA layout are evident.

The performance enhancement, however, is not achieved without cost: the number of phase delay degrees of freedom that must be corrected post-fabrication is increased from 7 to 14. Simulations suggest that the out-of-band crosstalk parameter is the most sensitive to residual errors in phase delays and coupling ratios, whereas the spectral shapes of the passbands are more robust. The transmission of QAM-16 data sets stringest

TABLE II
CHOICE OF PHASE DELAYS WITHIN CASCADED AUTO-REGRESSIVE
MOVING-AVERAGE FILTER MULTIPLEXER

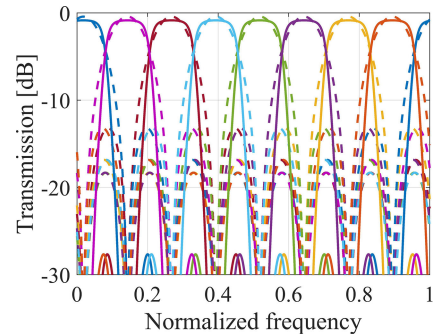| Filter unit	Differential phase delay	Phase delay in resonator
A	$\phi_A = 0$	$\phi_A^{(R)} = \pi$
B_1	$\phi_{B1} = 3\pi/2$	$\phi_{B1}^{(R)} = 0$
B_2	$\phi_{B2} = 0$	$\phi_{B2}^{(R)} = \pi$
C_1	$\phi_{C1} = 3\pi/4$	$\phi_{C1}^{(R)} = \pi/2$
C_2	$\phi_{C2} = \pi/4$	$\phi_{C2}^{(R)} = 3\pi/2$
C_3	$\phi_{C3} = \pi/2$	$\phi_{C3}^{(R)} = 0$
C_4	$\phi_{C4} = 0$	$\phi_{C4}^{(R)} = \pi$

Fig. 6. Calculated normalized-frequency transfer functions of the eight output ports of a wavelength-division multiplexing device, comprised of auto-regressive moving-average filter stages (solid lines). The corresponding transfer functions of a device consisted of cascaded Mach-Zehnder interferometers (Fig. 3) are shown for comparison (dashed lines).

crosstalk limitations: the relative power of interfering signals must be kept below -24 dB for a 1 dB pernalty at a bit error ratio of 1e-3 [35]. This requirement corresponds to residual errors of ± 0.1 rad in phase delays, and uncertainty of ± 0.1 in the values of the coupling parameter ρ.

Compared with most realizations of silicon-photonic multiplexing devices, the proposed layout is rather complex. The challenge of phase-delay adjustments is addressed by a one-time trimming protocol, as described next.

III. FABRICATION AND TUNING OF DEVICES

A. Device Fabrication

The silicon-photonic DWDM devices were fabricated by the commercial silicon foundry Tower-Jazz in Migdal Ha'Emek, Israel. Standard 8" SOI wafers were used. The thicknesses of the silicon device layer and the buried oxide layer were 220 nm and 2 μm, respectively. Ridge waveguides were defined in the silicon device layer using ultraviolet stepper photo-lithography, followed by an inductively-coupled plasma, reactive ion etching process. The waveguides were partially etched to 70 nm depth, and their width was 700 nm. The basic differential group delay unit τ was chosen as 15 ps (path imbalance of 1.3 mm). This
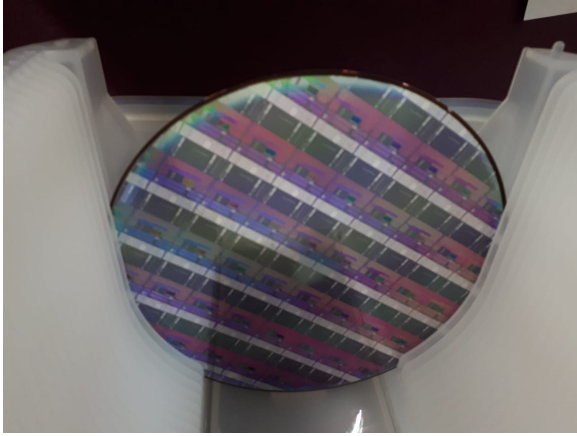
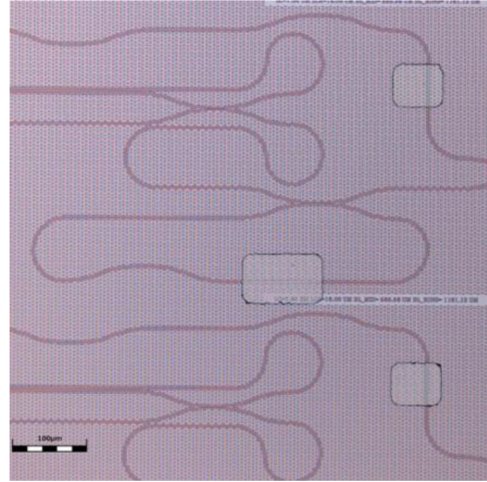Fig. 7. Image of a SOI wafer containing multiple wavelength-division multiplexer devices.

Fig. 8. Top optical microscope view of part of a fabricated eight-channel wavelength division multiplexer device (20× magnification). Patches of chalcogenide glass upper cladding may be seen on top of the waveguide paths, in three locations. The scale bar represents 100 μm.

delay corresponds to a channel spacing of 0.133 nm (17 GHz). The device layout included an input port, eight output ports, and test ports at the unused input ends of each MZI (see Fig. 4). Fig. 7 shows an image of a processed wafer. Wafers were diced into 1.2×1.2 cm^2 dies for subsequent processing and testing.

The directional couplers forming all MZI and resonator units were successfully fabricated to obtain the designed coupling ratios as described in Section II above, within tolerance and with no tuning required. The same holds for all group delays within MZIs and resonators. In contrast, the values of the critical phase delays were arbitrary. To allow for phase delay trimming, patches of photo-sensitive As$_2$Se$_3$ chalcogenide glass were deposited on top of the silicon-photonic waveguides, at selected locations [30], [31]: one on the longer arm of each MZI and one within each ring resonator (see Fig. 4).

The DWDM devices were first covered with a 10 nm-thick buffer layer of SiO$_2$ by ion beam sputtering from a silicon target. The deposition was performed at a pressure of 6.7e-4 mbar, and at 0.26 nm/s rate. The SiO$_2$ layer covered the entire surface of the sample. Lastly, regions of 150 nm-thick As$_2$Se$_3$ chalcogenide glass were defined by photo-lithography, thermal evaporation and lift-off. A bulk target was evaporated from a molybdenum boat at 1.3e-5 mbar pressure. The deposition rate was 0.5 nm/s. The chalcogenide cladding layer was sufficiently thin to prevent the leakage of light from the silicon core.

The refractive index of the chalcogenide cladding layer at 1550 nm wavelength is 2.8 refractive index units (RIU) [36]. Numerical simulations suggest that the effective index of the single transverse-electric (TE) mode of the silicon waveguide at the same wavelength is 2.85 RIU and 2.72 RIU, with and without the chalcogenide cladding, respectively. The chalcogenide cladding modifies the group delays of waveguide paths as well [30], [31]. In order to retain the proper ratios among group delays along different elements, the lengths of the chalcogenide cladding patches scaled with the group delay: from 50 μm in the *C*-stage MZIs (unit delay τ) to 400 μm over the ring resonator of the *A*-stage unit (delay of 8τ). Fig. 8 shows a top-view

microscope image of parts of a DWDM device, including three chalcogenide cladding patches.

B. Tuning of Phase Delays

Light was coupled in and out of the TE mode of devices under test using vertical grating couplers. Standard fibers were positioned above the grating couplers using six-axes positioning stages. The input fiber was moved between the main input port and the different test ports throughout the tuning procedure, and the output fiber was coupled to various output ports as necessary. Coupling losses of optical power between a standard optical fiber and the device under test were 10 dB at each end. Propagation losses along the waveguides were measured separately as 1.8 dB/cm.

Phase delays were adjusted by local illumination of the upper As$_2$Se$_3$ cladding. The device under test was exposed to the beam of a Ti:Sapphire ultrafast laser. The duration of the laser pulses was 200 fs, their repetition rate was 80 MHz, and the central wavelength was 810 nm. The average power of the pulses was controlled by a variable optical attenuator. The laser beam was focused on the surface of the device under test, to a spot-size diameter of 2 μm. A three-axes linear stage was used to scan the device, with input and output fibers in place, through the focused beam.

The two-photon absorption of the Ti:Sapphire laser light modifies the chalcogenide cladding layer through two mechanisms [32], [33]. When the illumination intensity is comparatively modest, the refractive index of the layer is locally increased due to a photo-darkening process [33]. The change in cladding index is on the order of 0.05-0.1 RIU [33], raising the local effective modal index by approximately 0.01 RIU [30], [31]. At higher intensity, a mass transfer effect takes place instead, locally removing the upper cladding layer altogether [30], [31]. In this case, the local effective index of the optical mode is reduced by 0.13 RIU.

Both mechanisms were used in the phase-delay trimming procedure: coarse adjustments through local mass transfer, and fine-tuning via photo-darkening. The intensity of the laser beam was 320 kW/cm^2 in the former process, and 160 kW/cm^2 in the latter. During illumination, the As$_2$Se$_3$-coated areas were translated through the focal point of the beam at 4 μm/s speed. The upper cladding patches were large enough to allow for several 2π cycles of phase delay adjustments, in cases of errors.

Phase delays within the seven filter units were corrected sequentially. The four C-stage filters were tuned first. The response of each unit was characterized using an optical vector network analyzer (OVNA) with a spectral resolution of 3 pm. Light was launched into the test port of the C-stage unit under test, and collected in one of its output ports. As noted in Section I above, the initial phase delays within the MZI and ring resonator following fabrication were arbitrary. The initial transfer function (Fig. 9(top), solid light green line) was therefore very different from the target response of the filter unit (dashed black trace). The actual values of the two phase delays within the unit were fitted based on the model of Section II.B, using offline processing. The necessary phase delay corrections were determined, and the motorized linear stages were programmed to scan waveguide segments of appropriate lengths through the laser writing beam. Waveguides were illuminated in discrete steps, and the transfer function was repeatedly measured following several such steps for validation purposes. Both MZI and ring were addressed during each step. The filter response was gradually adjusted from the arbitrary initial shape to that of a maximally-flat, ARMA bandpass filter (Fig. 9(top)).

Following the adjustment of the four C-stage filters, phase delays within the two intermediate B-stage units were trimmed next. The transfer function from a B-stage test port and an output of the entire device was measured using the OVNA (Fig. 9 (center)). Here too, the initial measured response was arbitrary. However, with the cascaded C-stages already tuned, the two phase delays within the B-stage unit under test could be retrieved based on the device model. Successive illumination steps gradually brought the measured response to its target shape. Note that the proper transfer function between the B-stage test port and the device output is not that of a de-multiplexer filter (Fig. 9 (center), dashed line). Lastly, the device response was measured between the common input and one of the outputs, and the two phases within the A-stage unit were adjusted using the same procedure (Fig. 9 (bottom)). The tuning of multiple elements did not introduce cross-interference: the illumination of a given upper cladding patch had no effect on any of the other phase delays.

Figure 10(top) shows OVNA measurements of the power transfer functions of all output ports, at the conclusion of the tuning procedure. A magnified view of the transfer functions within a single FSR is presented in Fig. 10(center). The input spectrum is divided in eight output channels with 0.133 nm spacing. The channels passbands are uniform, with full widths at half maximum of 0.11 nm. The wavelength-averaged out-of-band rejection is -28 dB, with worst-case crosstalk level of -22 dB. The spectral transitions between pass and stop bands
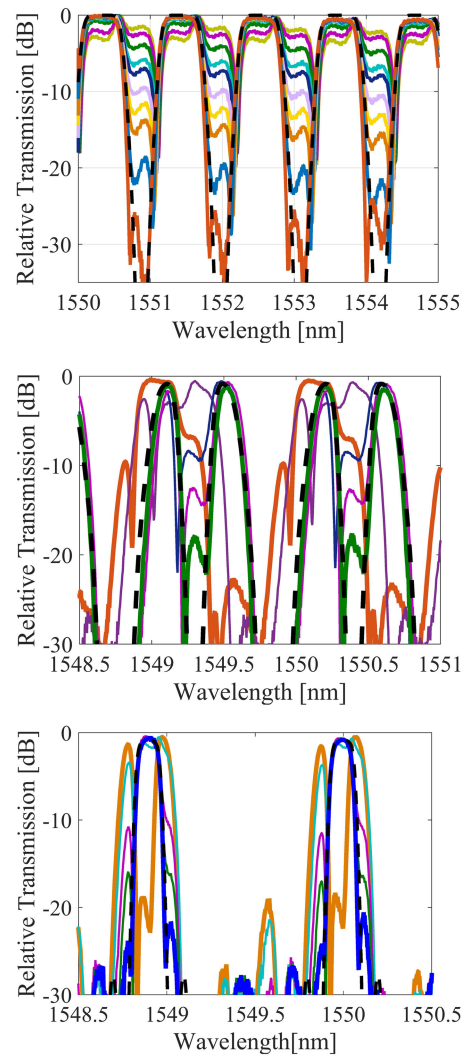

Fig. 9. Post-fabrication trimming of the relative power transfer functions. Top: Tuning the response of filter stage C_3, from its test port to output port 5 (see Fig. 4). Solid lines show measured transfer functions, starting from an arbitrary initial state (light green) to a final state that meets the design (orange). The dashed line shows the designed transfer function. Center: Tuning the response of filter stage B_2, from its test port to output port 5 (see Fig. 4). Solid lines show measured transfer functions, starting from an arbitrary initial state (orange) to a final state that meets the design (green). The dashed line shows the calculated transfer function from test port to output. Note that the response seen from the test port is not that of a de-multiplexer filter. Bottom: Tuning the response of filter stage A, from the common input port to output port 5. Solid lines show measured transfer functions, starting from an arbitrary initial state (orange) to a final state of an auto-regressive moving-average eight-channel de-multiplexer (blue). The dashed line shows the expected transfer function.

are considerably sharper than those of MZI-based DWDM devices, as expected.

The measured power transfer functions are in very good agreement with design (Fig. 10(bottom)). The figure also shows the measured and calculated group delays of a single output, within a single passband. Group delay variations of 40 ps are observed between the band edges and the central transmission wavelength. Measured group delays are in very good agreement with productions. End-to-end in-band transmission losses were -22 dB. Losses were dominated by input and output coupling at
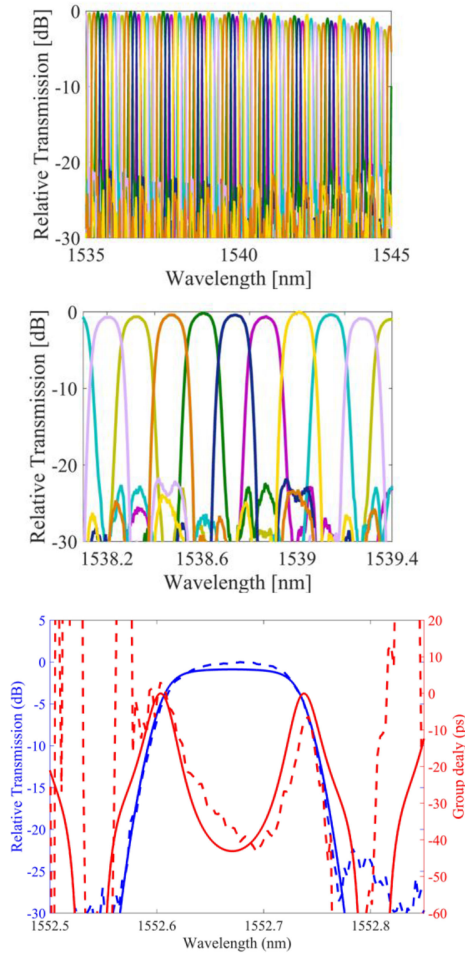
Fig. 10. Top: Measured relative power transfer functions of all eight output ports of a silicon-photonic dense wavelength-division multiplexer device. Center: magnified view of the transfer functions within a single free spectral range. Bottom: Magnified view of a single pass-band of one output port. Blue traces present relative power transfer functions (left vertical axis). Red traces show relative group delay variations (right vertical axis). The designed response is noted in solid lines, and measurements are shown in dashed traces.
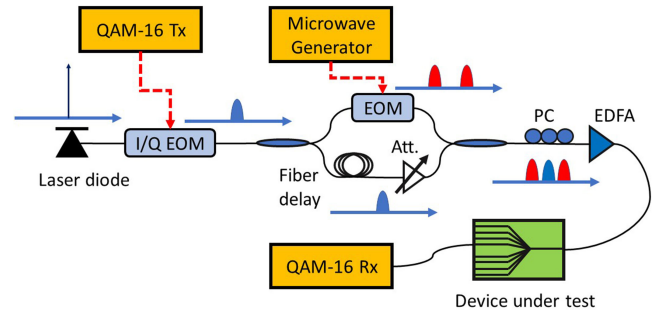

Fig. 11. Schematic illustration of the experimental setup used in the de-multiplexing of three data channels. EOM: electro-optic modulator. PC: polarization controller. EDFA: erbium-doped fiber amplifier. Att.: variable attenuator. QAM: quadrature amplitude modulation. Tx: transmitter. Rx: Receiver.
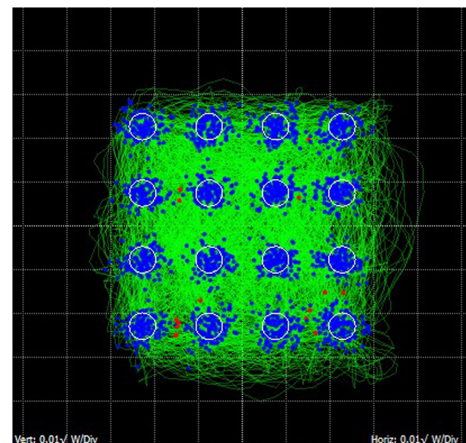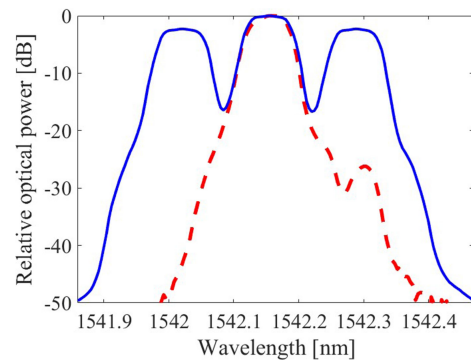

Fig. 12. Top, blue solid trace: Relative power spectral density of three optical communication channels at the input of a silicon-photonic wavelength-division multiplexer. Each channel carried 40 Gbit/s data at QAM-16 format. The spacing between the optical carrier frequencies of the three channels was 17 GHz. Dashed red trace: relative power spectral density of the waveform at the output port of the device that corresponds to the central channel. The outer channels were suppressed by at least 25 dB. Bottom: Constellation diagram of QAM-16 data of the central optical channel following de-multiplexing. The measured bit error ratio in 1 million bits was 5e-4. The average error vector magnitude in a block size of 10,000 bits was 0.105.

the vertical gratings. The coupling losses are not fundamental, and may be reduced if fibers are permanently fixed to the device under test. The high quality of the periodic transfer functions is retained over a 10 nm-wide bandwidth, limited by residual imbalance of group delays.

IV. DE-MULTIPLEXING OF DATA CHANNELS

Figure 11 illustrates the measurement setup used in the de-multiplexing of adjacent wavelength-division communication channels. Light from the output of a distributed feedback laser diode at 1542.15 nm wavelength was modulated by QAM-16 data, at 10 Gbd/s rate (40 Gbit/s). The data-carrying optical waveform was split into two paths. The signal in the lower branch served as a central communication channel. Light in the upper branch passed through an electro-optic amplitude modulator that was biased for carrier suppression, and driven by a sine-wave at 17 GHz frequency from the output of a microwave generator. The modulation generated two replicas of the

data-carrying channel, at central optical frequencies that were 17 GHz above and below that of the original one.

The two outer communication channels were recombined with the central channel by an optical coupler (see Fig. 11). The waveform in the lower path was delayed over few meters of fiber, so that data in the central channel were uncorrelated with those in the outer two. A variable optical attenuator was

used to equalize the power levels of the three channels to within 2 dB. Fig. 12(top, blue trace) shows the normalized optical power spectral density of the three channels combined. The spectral efficiency of data transmission was 2.35 bit/s per Hz. In a control experiment, the combined waveform was directly connected to the optical input port of a QAM-16 receiver. Without channel de-multiplexing, the receiver could not identify the data transmission pattern due to inter-channel interference.

The combined three channels were then coupled to the input port of the device under test. The overall power level at the input fiber was 16 dB (approximately 6 dBm coupled into the chip). The device temperature was maintained at 25 ± 0.001 °K. Fig. 12(top, red trace) shows the normalized optical power spectral density at the output port corresponding to the central channel. The two outer channels were suppressed by at least 25 dB. Lastly, Fig. 12(bottom) shows the detected QAM-16 constellation diagram of the de-multiplexed central channel. The measured bit error ratio in 1 million bits was 5e-4, well within the specifications for forward error correction. The average error vector magnitude of the 16 symbols over a block size of 10,000 bits was 0.105. No electronic filters were used in the detection scheme.

V. CONCLUSION

An eight-channel DWDM silicon-photonic device based on cascaded ARMA filter stages was designed, fabricated and tested. Compared with most previous realizations, the device layout is comparatively complex. In return, however, the response of the device is characterized by ultra-narrow channel spacing of only 0.133 nm (17 GHz), highly uniform passbands, strong out-of-band rejection and sharp spectral transitions. The proper functioning of the device requires precise control over 14 phase delays. One-time trimming of these delays was achieved through the local illumination of upper cladding regions of photo-sensitive chalcogenide glass. Individual phase-delay degrees of freedom could be adjusted with no cross-interference effects. The de-multiplexing of three adjacent 16-QAM, 40 Gbit/s wavelength-division channels, with a spectral efficiency of 2.35 bit/s per Hz in a single polarization, was successfully demonstrated.

The tuning process is suitable for automation: The transfer function of a filter unit under study is measured following every illumination step, phase delays are fitted using a numerical model, and the next trimming step is defined accordingly. The response of the device was tested over several months following fabrication, with negligible changes. The device, however, must be packaged and kept away from exposure to ambient light during service, to prevent unintended phase delay modifications.

Due to the large thermo-optic coefficient of silicon and the dense channels spacing, the alignment of transfer functions with the absolute wavelengths of the input data requires the stabilization of device temperature to within several milli- Kelvin. Note that the thermo-optic coefficient of the chalcogenide glass upper cladding is smaller than that of silicon. Hence the temperature control requirements of most silicon-photonic devices with comparable channels spacing would be similar. Post-fabrication trimming of phase delays is required in many other silicon-

photonic devices, such as AWGs. The protocol described in this work is applicable to those devices as well. Lastly, arsenic-free chalcogenide glass compositions, such as gallium-lanthanum-sulfide (GLS) [37], may be used as alternative photo-sensitive upper cladding materials in future studies.

Due to the relative layout complexity, access to a commercial silicon foundry was central to the fabrication success. The proposed DWDM devices are applicable to data center communications, as well as chip-level all-optical filtering of mobile communication waveforms and radio-over-fiber signals [38], [39]. Future work would include additional data transfer experiments, scaling of devices to larger channel counts, and the development of a fully-automated trimming process.

REFERENCES

[1] G. T. Reed, *Silicon Photonics: The State of the Art*. Hoboken, NJ, USA: Wiley, 2008.

[2] L. Vivien and L. Pavesi Eds., *Handbook of Silicon Photonics*. New York, NY, USA: Taylor & Francis, 2016.

[3] D. A. B. Miller, "Device requirements for optical interconnects to silicon chips," *Proc. IEEE*, vol. 97, no. 7, pp. 1166–1185, Jul. 2009.

[4] Y. A. Vlasov, "Silicon CMOS-integrated nano-photonics for computer and data communications beyond 100 G," *IEEE Commun. Mag.*, vol. 50, no. 2, pp. S67–S72, Feb. 2012.

[5] W. Bogaerts *et al.*, "Silicon-on-insulator spectral filters fabricated with CMOS technology," *IEEE J. Sel. Topics in Quantum Electron.*, vol. 16, no. 1, pp. 33–44, Jan./Feb. 2010.

[6] D. Dai and J. E. Bowers, "Silicon-based on-chip multiplexing technologies and devices for Peta-bit optical interconnects," *Nanophotonics*, vol. 3, no. 4/5, pp. 283–311, 2014.

[7] F. Horst *et al.*, "Cascaded Mach-Zehnder wavelength filters in silicon photonics for low loss and flat pass-band WDM (de-)multiplexing," *Opt. Express*, vol. 21, no. 10, pp. 11652–11658, May 2013.

[8] S.-H. Jeong *et al.*, "Low-loss, flat-topped and spectrally uniform silicon-nanowire-based 5th-order CROW fabricated by ArF-immersion lithography process on a 300-mm SOI wafer," *Opt. Express*, vol. 21, no. 25, pp. 30163–30174, Dec. 2013.

[9] T. Fukazawa, F. Ohno, and T. Baba, "Very compact arrayed-waveguide-grating demultiplexer using Si photonic wire waveguides," *Japanese J. Appl. Phys.*, vol. 43, no. 5B, pp. L673–L675, 2004.

[10] P. Cheben *et al.*, "A high-resolution silicon-on-insulator arrayed waveguide grating microspectrometer with submicrometer aperture waveguides," *Opt. Express*, vol. 15, pp. 2299–2306, Mar. 2007.

[11] S. Pathak, M. Vanslembrouck, P. Dumon, D. Van Thourhout, and W. Bogaerts, "Optimized silicon AWG with flattened spectral response using an MMI aperture," *J. Lightw. Technol.*, vol. 31, no. 1, pp. 87–93, Jan. 2013.

[12] S. Cheung, T. Su, K. Okamoto, and S. J. B. Yoo, "Ultra-compact silicon photonic 512×512 25 GHz arrayed waveguide grating router," *IEEE J. Sel. Topics Quantum Electron.*, vol. 20, no. 4, Jul./Aug. 2014, Art. no. 8202207.

[13] S. Pathak, P. Dumon, D. Van Thourhout, and W. Bogaerts, "Comparison of AWGs and Echelle gratings for wavelength division multiplexing on silicon-on-insulator," *IEEE Photon. J.*, vol. 6, no. 5, Oct. 2014, Art. no. 4900109.

[14] J. Brouckaert, W. Bogaerts, P. Dumon, D. Van Thourhout, and R. Baets, "Planar concave grating demultiplexer fabricated on a nanophotonic silicon-on-insulator platform," *J. Lightw. Technol.*, vol. 25, no. 5, pp. 1269–1274, May 2007.

[15] F. Horst, W. M. J. Green, B. Offrein, and Y. Vlasov, "Silicon-on-insulator echelle grating WDM demultiplexers with two stigmatic points," *IEEE Photon. Technol. Lett.*, vol. 21, no. 23, pp. 1743–1745, Dec. 2009.

[16] X. Pommarede *et al.*, "16 times 100 GHz Echelle grating-based wavelength multiplexer on silicon-on-insulator platform," *IEEE Photon. Technol. Lett.*, vol. 29, no. 6, pp. 493–495, Mar. 2017.

[17] H. Lira, S. Manipatruni, and M. Lipson, "Broadband hitless silicon electrooptic switch for on-chip optical networks," *Opt. Express*, vol. 17, no. 25, pp. 22271–22280, Nov. 2009.

[18] S. Ibrahim *et al.*, "Demonstration of a fast-reconfigurable silicon CMOS optical lattice filter," *Opt. Express*, vol. 19, no. 14, pp. 13245–13256, Jun. 2011.

[19] P. Dong *et al.*, "Thermally tunable silicon racetrack resonators with ultralow tuning power," *Opt. Express*, vol. 18, no. 19, pp. 20298–20304, Sep. 2010.

[20] J. Sun, E. Timurdogan, A. Yaacobi, E. S. Hosseini, and M. R. Watts, "Large-scale nanophotonic phased array," *Nature*, vol. 493, no. 7431, pp. 195–199, Jan. 2013.

[21] L. Zhou, K. Okamoto, and S. J. B. Yoo, "Athermalizing and trimming of slotted silicon microring resonators with UV-sensitive PMMA uppercladding," *IEEE Photon. Technol. Lett.*, vol. 21, no. 17, pp. 1175–1177, Sep. 2009.

[22] S. Lambert, W. De Cort, J. Beeckman, K. Neyts, and R. Baets, "Trimming of silicon-on-insulator ring resonators with a polymerizable liquid crystal cladding," *Opt. Lett.*, vol. 37, no. 9, pp. 1475–1477, May 2012.

[23] J. Schrauwen, D. Van Thourhout, and R. Baets, "Trimming of silicon ring resonator by electron beam induced compaction and strain," *Opt. Express*, vol. 16, no. 6, pp. 3738–3743, Mar. 2008.

[24] A. H. Atabaki, A. A. Eftekhar, M. Askari, and A. Adibi, "Accurate postfabrication trimming of ultracompact resonators on silicon," *Opt. Express*, vol. 21, no. 12, pp. 14139–14145, Jun. 2013.

[25] C. K. Madsen and J. H. Zhao, *Optical Filter Design and Analysis – A Signal Processing Approach*. Hoboken, NJ, USA: Wiley, 1999.

[26] S.-H. Jeong *et al.*, "Flat-topped and low loss silicon-nanowire-type optical MUX/DeMUX employing multi-stage microring resonator assisted delayed Mach-Zehnder interferometers," *Opt. Express*, vol. 20, no. 23, pp. 26000–26011, Nov. 2012.

[27] S.-H. Jeong, Y. Tanaka, and K. Morito, "1 × 4 channel Si-Nanowire microring-assisted multiple Delayline-Based optical MUX/DeMUX," *J. Lightw. Technol.*, vol. 33, no. 17, pp. 3736–3743, Sep. 2015.

[28] J. Cardenas *et al.*, "Linearized silicon modulator based on a ring assisted Mach Zehnder inteferometer," *Opt. Express*, vol. 21, no. 19, pp. 22549–22557, Sep. 2013.

[29] A. Canciamilla *et al.*, "Photo-induced trimming of chalcogenide-assisted silicon waveguides," *Opt. Express*, vol 20, no. 14, pp. 15807–15817, 2012.

[30] R. Califa *et al.*, "Large photo-induced index variations in chalcogenide-on-silicon waveguides," *Opt. Lett.*, vol. 39, no. 20, pp. 5905–5908, Oct. 2014.

[31] R. Califa *et al.*, "Large one-time photo-induced tuning of directional couplers in chalcogenide-on-silicon platform," *Opt. Express*, vol. 23, no. 22, pp. 28234–28243, Oct. 2015.

[32] A. E. Owen, A. P. Firth, and P. J. S. Ewen, "Photo-induced structural and physico-chemical changes in amorphous chalcogenide semiconductors," *Philos. Mag. Part B*, vol. 52, no. 3, pp. 347–362, 1985.

[33] A. Zoubir *et al.*, "Direct femtosecond laser writing of waveguides in As_2S_3 thin films," *Opt. Lett.*, vol. 29, no. 7, pp. 748–750, Apr. 2004.

[34] D. Munk *et al.*, "Silicon-photonic dense 8-channel multiplexer using autoregressive moving-average filters," in *Proc. IEEE Microw. Photon. Conf.*, Toulouse, France, Oct. 2018, pp. 1–4.

[35] P. Winzer, A. Gnauck, A. Konczykowska, F. Jorge, and J. Y. Dupuy, "Penalties from in-band crosstalk for advanced optical modulation formats," in *Proc. Eur. Conf. Expo. Opt. Commun.*, Sep. 2011, pp. 1–3.

[36] M. D. Pelusi *et al.*, "Applications of highly-nonlinear chalcogenide glass devices tailored for high-speed all-optical signal processing," *IEEE J. Sel. Topics Quantum Elect.*, vol. 14, no. 3, pp. 529–539, May/Jun. 2008.

[37] J. A. Frantz *et al.*, "Sputtered films of Er3+-doped gallium lanthanum sulfide glass," *Mater. Lett.*, vol. 60, no. 11, pp. 1350–1353, May 2006.

[38] D. Marpaung *et al.*, "Integrated microwave photonics," *Laser Photon. Rev.*, vol 7, no. 4, pp. 506–538, Jul. 2013.

[39] D. Novak *et al.*, "Radio-over-fiber technologies for emerging wireless systems," *IEEE J. Quantum Electron.*, vol. 52, no. 1, Jan. 2016, Art. no. 0600311.

Dvir Munk received the B.Sc. and M.Sc. degrees in electrical engineering from Bar-Ilan University, Ramat Gan, Israel, in 2013 and 2015, respectively, where he is currently working toward the Ph.D. degree in electrical engineering.

His research interests include silicon photonics, optical communication, and nonlinear and opto-mechanical propagation effects in photonic integrated circuits.

Moshe Katzman received the B.Sc. and M.Sc. degrees in electrical engineering from Bar-Ilan University, Ramat Gan, Israel, in 2015 and 2017, respectively, where he is currently working toward the Ph.D. degree in electrical engineering.

His research interests include the development of hybrid-silicon photonics fabrication and measurements techniques, nonlinearities of chalcogenide glasses, and surface acoustic wave in silicon photonics.

Yuri Kaganovskii received the M.Sc. degree in solid-state physics in 1964, the Ph.D. degree in crystallography and crystal physics in 1970, and the D.Sci degree in solid-state physics in 1984, all from the Kharkov State University, Kharkiv, Ukraine.

From 1969 to 1988, he was a Senior Research Scientist with the Department of Crystal Physics, Kharkov State University, and from 1988 to 1995, he was a Professor with the same department. Since 2000, he has been an Associate Professor with the Department of Physics, Bar-Ilan University, Israel. He is the author of one monograph, more than 170 articles, and five inventions. His research interests include diffusion in solids, surface phenomena, photoinduced phenomena and mass transfer in thin solid films, light scattering at solids surfaces, and laser microfabrication.

Dr. Kaganovskii is a member of the Editorial Board of *Materials Letters* journal. He was the recipient of the scientific awards of the Ministry of Higher and Secondary Special Education of the USSR, and the *Inventor of the USSR* medal from the USSR Committee.

Naor Inbar received the B.Sc. degree in biotechnology and food engineering from the Technion–Israel Institute of Technology, Haifa, Israel, in 1999. He completed his studies in micro-electronics fabrication process engineering with the Technion, in 2001.

Since 2001, he held several engineering positions with semiconductor industry companies in Israel. Since 2010, He has been a Research and Development Engineer with Tower-Jazz semiconductors, Migdal Ha'Emek, Israel.

Arijit Misra received the M.Sc. degree in physics from the Indian Institute of Engineering, Science and Technology, Shibpur, Howrah, India, in 2015. He was a Research Assistant with the Centre for Nano-Electro-Mechanical Systems and Nanophotonics, Indian Institute of Technology, Madras before joining the Institute for High-Frequency Technology, TU Braunschweig, Germany in 2017 as a Ph.D. student. His research interest includes integrated photonic devices design, fabrication, and characterization, and their application to optical signal processing.

Mirit Hen received the B.Sc., M.Sc. and Ph.D. degrees in chemistry from Bar-Ilan University, Ramat Gan, Israel, in 2009, 2012, and 2017, respectively.

From 2016 to 2018, she was a Postdoctoral Research Fellow with the Faculty of Engineering, Bar-Ilan University. Since 2018, she has been a Staff Scientist with the same faculty. Her research interests includes surface chemistry, organic chemistry, and fabrication of photonic devices in silicon and glass.

Dr. Hen was the recipient of the Academia-Industry Fellowship for the Promotion of Women in Science from the Israeli Ministry of Science, Technology, and Space in 2017.

Maayan Priel received the B.Sc. and M.Sc. degrees in chemistry with Bar-Ilan University, Ramat Gan, Israel. She is currently working toward the Ph.D. degree in electrical engineering with the same University.

Her current research includes fabrication and measurements of passive and active photonic devices, in silicon and in erbium-doped crystals.

Moshe Feldberg received the practical electrical engineering degree from Tel-Aviv University, Tel Aviv, Israel, in 1988.

From 1988 to 2009, he was as a Research and Development Engineer for several ASIC companies. He managed research groups in Intel, M-Systems/SanDisk, Motorola semiconductors, Tower Semiconductor, Metalink & ISD. Since 2009, he manages the device fabrication facilities of the Bar-Ilan University Institute for Nano-Technology and Advanced Materials (BINA), Ramat-Gan, Israel, as a Staff Scientist.

He was the recipient of the Intel Outstanding Employee Award for his contribution to the 80860XP Processor, and was named M-Systems/SanDisk Employee of the Year four times.

Maria Tkachev received the B.Sc. degree in materials engineering from the Technion—-Israel Institute of Technology, Haifa, Israel, in 1996. She received the M.Sc. and Ph.D. degrees in chemical physics from the Weizmann Institute of Science, Rehovot, Israel, in 2007 and 2014, respectively.

Since 2017, she has been working as a Research Scientist with of the Bar-Ilan University Institute for Nano-Technology and Advanced Materials, Ramat-Gan, Israel.

Arik Bergman (M' 17) received the B.Sc., M.Sc. and Ph.D. degrees in electrical engineering from Tel-Aviv University, Tel Aviv, Israel, in 2006, 2011, and 2017, respectively.

Since 2016, he has been a Postdoctoral Research Fellow with the Faculty of Engineering, Bar Ilan University, Ramat-Gan, Israel. His research interests include opto-mechanical interactions in integrated photonic devices and fibers, Brillouin lasers, phononic oscillators, and fiber imaging and sensor systems.

Menachem (Nachi) Vofsi received the B.Sc. degree in physics from the Technion—-Israel Institute of Technology, Haifa, Israel, in 1983, and the M.Sc. degree in solid state physics from the same institute in 1986. He received the MBA degree with Herriot Watt University, Edenborough, U.K., in 1998.

He joined Tower-Jazz Semiconductors, Migdal Ha'Emek, Israel, in 1986, where he is currently the Director of Research and Development.

Michael Rosenbluh was born in Budapest, Hungary, in 1949, and received the Ph. D. degree in physics from the Massachusetts Institute of Technology (MIT), Cambridge, MA, USA, in 1978. His doctoral research was in experimental laser spectroscopy, in particular the exploration of the effects of very high magnetic fields on the spectroscopy of atomic helium.

He continued as a Research Staff Member of the MIT Francis Bitter National Magnet Laboratory until 1980, when he joined the Physics Faculty of Bar-Ilan University, Ramat Gan, Israel. Since 1992, he has been a Full Professor with Bar-Ilan and was a Chairman with the Physics Department from 2011 to 2017.

Through his academic career, he has been a Visiting Scientist and a Professor at various locations in the USA. In the 80's, he was associated with the MIT Magnet Lab and MIT Lincoln Laboratory. In 1990, he was a Visiting Scientist with IBM Almaden Research Lab, Almaden, CA, USA. He has also been a Visiting Professor on a number of occasions with the National Institute of Standards and the University of Colorado, Boulder, CO, USA. He has authored or coauthored more than 150 articles in refereed journals in these areas. His main research focus has remained in laser spectroscopy and quantum optics.

Thomas Schneider received the Diploma in electrical engineering from the Humboldt Universität zu Berlin, Berlin, Germany, in 1995, and the Ph.D. degree in physics from the Brandenburgische Technische Universität Cottbus, Cottbus, Germany, in 2000.

From 2000 to 2013, he was with the Deutsche Telekom Hochschule für Telekommunikation (HfT), Leipzig, Germany. From 2006 to 2013, he was the Head of the Institut für Hochfrequenztechnik, HfT. Since 2014, he has been the Head of the Terahertz Photonics Group, Institut für Hochfrequenztechnik, Technische Universität Braunschweig, Germany. His current research interests include nonlinear optical effects in telecommunication systems and sensors, slow and fast light, high resolution spectroscopy, the generation of millimeter and THz waves, optical sampling, and integrated photonics.

Avi Zadok received the B.Sc. degree in physics and mathematics from the Hebrew University of Jerusalem, Jerusalem, Israel, in 1994, the M.Sc. degree in physical electronics from Tel-Aviv University, Tel Aviv, Israel, in 1999, and the Ph.D. degree in electrical engineering from the same University in 2007.

From 2007 to 2009, he was a Postdoctoral Research Fellow with the Department of Applied Physics, California Institute of Technology. In 2009, he joined the Faculty of Engineering, Bar-Ilan University, Israel, where he is a Full Professor since 2017. He is the Co-Author of 140 papers in scientific journals and proceedings of international conferences. His research interests include fiber-optics, nonlinear optics, integrated photonic devices, and opto-mechanics.

Dr. Zadok was the recipient of the Krill Award of the Wolf Foundation in 2013. He was also the recipient of a Starter Grant from the European Research Council in 2015. He is a member of the Israel Young Academy, and serves in its Steering Committee.